

## CuO nanoparticles as copper-ion reservoirs for Elesclomol-mediated intracellular oxidative stress

Chakraborty, Swaroop; Prakash, Prabhat; Shah, Juhi; Mayya, Chaithra; Singh, Sanjay; Ranganathan, Raghavan; Soppina, Virupakshi; Jones, Eugenia Valsami; Misra, Superb K.

DOI:

[10.1021/acsnm.1c04350](https://doi.org/10.1021/acsnm.1c04350)

License:

None: All rights reserved

*Document Version*

Peer reviewed version

*Citation for published version (Harvard):*

Chakraborty, S, Prakash, P, Shah, J, Mayya, C, Singh, S, Ranganathan, R, Soppina, V, Jones, EV & Misra, SK 2022, 'CuO nanoparticles as copper-ion reservoirs for Elesclomol-mediated intracellular oxidative stress: implications for anticancer therapies', *ACS Applied Nano Materials*, vol. 5, no. 1, pp. 1607-1620. <https://doi.org/10.1021/acsnm.1c04350>

[Link to publication on Research at Birmingham portal](#)

### **Publisher Rights Statement:**

This document is the Accepted Manuscript version of a Published Work that appeared in final form in ACS Applied Nano Materials, copyright © American Chemical Society after peer review and technical editing by the publisher. To access the final edited and published work see: <https://doi.org/10.1021/acsnm.1c04350>

### **General rights**

Unless a licence is specified above, all rights (including copyright and moral rights) in this document are retained by the authors and/or the copyright holders. The express permission of the copyright holder must be obtained for any use of this material other than for purposes permitted by law.

- Users may freely distribute the URL that is used to identify this publication.
- Users may download and/or print one copy of the publication from the University of Birmingham research portal for the purpose of private study or non-commercial research.
- User may use extracts from the document in line with the concept of 'fair dealing' under the Copyright, Designs and Patents Act 1988 (?)
- Users may not further distribute the material nor use it for the purposes of commercial gain.

Where a licence is displayed above, please note the terms and conditions of the licence govern your use of this document.

When citing, please reference the published version.

### **Take down policy**

While the University of Birmingham exercises care and attention in making items available there are rare occasions when an item has been uploaded in error or has been deemed to be commercially or otherwise sensitive.

If you believe that this is the case for this document, please contact [UBIRA@lists.bham.ac.uk](mailto:UBIRA@lists.bham.ac.uk) providing details and we will remove access to the work immediately and investigate.

# CuO Nanoparticles as Copper Ion Reservoirs for Elesclomol-Mediated Intracellular Oxidative Stress: Implications for Anticancer Therapies

*Swaroop Chakraborty<sup>\*a,b</sup>, Prabhat Prakash<sup>a</sup>, Juhi Shah<sup>c</sup>, Chaithra Mayya<sup>d</sup>, Sanjay Singh<sup>c</sup>  
Raghavan Ranganathan<sup>a</sup>, Virupakshi Soppina<sup>d</sup>, Eugenia Valsami Jones<sup>b</sup>, Superb K. Misra<sup>a\*</sup>*

<sup>a</sup>Materials Engineering, Indian Institute of Technology Gandhinagar, Gandhinagar, India, 382355

<sup>b</sup>School of Geography, Earth & Environmental Sciences, University of Birmingham, UK, B152TT

<sup>c</sup>Division of Biological and Life Sciences, Ahmedabad University, Ahmedabad, India, 380009.

<sup>d</sup>Biological Engineering, Indian Institute of Technology Gandhinagar, Gandhinagar, India, 382355

KEYWORDS: Dissolution; Oxidative stress; Elesclomol; nanoparticles; Tracing; Molecular dynamics; DFT

## ABSTRACT

Dissolution of metal/metal oxide nanoparticles has been widely exploited to be one of the mechanisms of inducing oxidative stress within the bacterial and mammalian cells. Elesclomol has been already evaluated in clinical trials, and the reports have demonstrated a greater therapeutic activity with a prolonged progression-free time for survival of patients. Computational modeling (DFT and classical molecular dynamics) and UV-Vis spectroscopy analysis showed that the dissolved Cu (II) ions from CuO nanoparticles preferentially bind to Elesclomol in cell culture media. CuO nanoparticles (50-200 ng/mL) when co-delivered with 50 ng/mL of Elesclomol drug significantly reduced the cell viability of A549 cells compared to their respective standalone exposure. A time dependent study showed a reduced cell viability (up to 80%) and enhanced ROS generation (up to 3 folds), which was explained by the dissolution profile of CuO nanoparticles. Stable isotope tracing confirmed the intracellular accumulation of copper inside A549 cells to increase by up to 4 times when 1000 ng/mL  $^{65}\text{CuO}$  nanoparticles were exposed in presence of 50 ng/mL Elesclomol. The cytotoxicity was rapid, with 70% of the cells death occurring within the span of 12 h through apoptosis pathways with a very minimal drug concentration. In our work, we exploited the ability of CuO nanoparticles to act as a reservoir with slow and sustained release of Cu (II) ions to bind with Elesclomol, which helped in enhanced generation of intracellular oxidative stress and can be used as a promising approach for Elesclomol based anticancer therapy.

## 1. INTRODUCTION

Cancer is known to be one of the primary causes of death and has become one of the major health concerns worldwide. The cancer is generally characterized by abnormal growth and proliferation of cells. Currently, there are several treatment options available for cancer such as surgery, chemotherapy, radiotherapy etc., yet the use of such intervention in general becomes unaffordable and causes side effects that leads to reduction in the use of cancer treatment options. Due to these limitations, there is a requirement of effective, inexpensive, and biocompatible intervention that can be affordable, high efficacy in the treatment. One such approach is ROS mediated oxidative therapy. The cancer cells are adapted to oxidative stress through several known mechanisms that allow them to survive in hypoxic conditions and become resistant to various anticancer drugs. However, when the ROS production exceeds the threshold, it can lead to death of cancer cells.

Metal oxide nanoparticles such as CuO, ZnO etc. have been reported to induce cell death via inducing oxidative stress inside the cells. These metal oxide nanoparticles induce cancer cell death through the mechanism such as “Trojan Horse”, and “Fenton reaction”<sup>1</sup>. The dissolution of metal/metal oxide nanoparticles has been widely exploited to be one of the mechanisms of inducing oxidative stress within the bacterial and mammalian cells. The oxidative stress is facilitated by an enhanced release of metal ions in biological milieu and interfering with the electron transport chain within mitochondria to generate dissolved ionic species<sup>2</sup>. The alternation of ATP production pathways results in enhanced production of ROS inside mitochondria. Cancer cells adapt to such high ROS production and gets resistant to majority of chemotherapeutic drugs. However, uncontrolled ROS production beyond threshold in a cancer cell can be a potential target for oxidative therapy<sup>3</sup>.

Elesclomol (1-N', 3-N'-bis (benzenecarbonothioyl) - 1 -N', 3-N'-dimethylpropanedihydrazide) triggers the anticancer activities by increasing the production of ROS and subsequently activating the apoptotic pathway. Elesclomol has been already evaluated in clinical trials, and the reports have demonstrated a greater therapeutic activity with a prolonged progression-free time for the survival of the patient<sup>6</sup>. The functioning of Elesclomol drug is elicited by its high binding affinity to copper (II) ions and selectively transports copper (II) ions to mitochondria and creates an alteration in the electron transport chain<sup>7</sup>. Elesclomol binds with Cu (II) ions and forms a neutral complex. According to the X-ray structure reported by Yadav et al (2013), the bivalent Cu binds to Elesclomol through the loss of two protons from the N1 and N2 atoms of Elesclomol molecules and forms a neutral complex. The Elesclomol drug has a significantly high affinity towards copper (II) ions with a binding affinity value of  $10^{24.1} \text{ M}^{-1}$ . The bonding of Cu (II) is very strong with Elesclomol and it is expected to have a slow dissociation of Cu (II) from the complex. Research results have reported that Cu-Elesclomol complexes are 1040 folds and 34 folds more potent than Pt-Elesclomol complex and Ni-Elesclomol complex respectively in reducing the cell viability of K562 cells<sup>8</sup>. The author demonstrated a high efficacy of Cu ion as a redox metal to kill the cancer cells when it forms complex with Elesclomol drug<sup>8</sup>. As shown in Figure 1, the free Elesclomol drug makes a stable complex with Cu (II) ions by donating four lone pairs and that makes the complex more hydrophobic in nature. Such enhancement in hydrophobicity increases the uptake of Cu-Elesclomol complex by the cells and hence more amount of Cu (II) enters the mitochondria to enhance the ROS production<sup>7</sup>. Nagai et al.<sup>7</sup> demonstrated the efficacy of Elesclomol drug to chelates free Cu (II) ions and selectively transfer Cu ions to mitochondria and induces oxidative stress in cancer cells. The dissociation of Cu (II) ions from Elesclomol occurs because of a highly reducing environment of mitochondria. As shown in Figure 1, The reducing groups like ascorbic

acid plays a major role in reducing Cu (II) to Cu (I). Since Elesclomol can only form complexes with Cu (II), the reduced Cu (I) immediately disassociates with the complex and that makes Elesclomol available freely to complex with other available free Cu (II) ions. The previously reported work mainly discussed the delivery of Cu (II)-Elesclomol complex to the cells at a certain concentration to induce oxidative stress. It was identified that the bioavailability of Cu (II) ions acts as a limiting factor because once the Elesclomol delivers the Cu (II) ions inside the cells, the drug molecules effluxes out from the cells to form complex other available free Cu ions. However, the free Cu ions are not readily available in the extracellular matrix because they form organic/inorganic complex.

In addition to experimental methods, computer simulations are widely used a tool to model drug-metal ion binding and spectral elucidation<sup>9, 10</sup>. While molecular dynamics (MD) based simulations are performed to understanding atomic scale interactions in condensed phase of the drug-ion binding, a detailed and more accurate information about the energetics and spectra can be extracted from quantum mechanics based density functional theory (DFT) calculations<sup>11,12</sup>. In case of metal ion-drug environment, competitive interaction of the metal ion with the drug *vs.* the constituents of medium affect the binding affinity. Since dissolution media like DMEM contains various amino acids, their cooperative effects on drug-ion binding dictate the extent of binding. The relative affinity of metal ion for amino acids *vs.* drug or among amino acids can be modeled using DFT calculations. In our study, we are using CuO nanoparticles as the reservoir to maintain a sustained release of Cu (II) ions until the nanoparticles are completely dissolved in the biological media. The slow and sustained release of Cu (II) ions will provide a time lag to Elesclomol molecules to capture other free Cu (II) ions and deliver it inside mitochondria. The process helps in reducing the dosage requirement of Elesclomol and CuO nanoparticles because of their synergistic effect in

inducing oxidative stress and can be a promising approach towards enhanced oxidative stress based anticancer therapy.

## **2. MATERIALS AND METHODS**

**2.1 Materials.** All the chemicals used for conducting the experiments were of analytical grade.  $\text{CuCl}_2 \cdot 2\text{H}_2\text{O}$ , NaOH and acetic acid was procured from Himedia Ltd, India.  $^{65}\text{CuCl}_2$  was obtained from Trace sciences International, USA. The biological assays i.e. MTT, Annexin V, DCFDA, mitochondrial membrane potential assay kit, ROS assay kit were obtained from Sigma Aldrich, USA. The Inductively Coupled Plasma-Mass Spectroscopy (ICP-MS) standards were procured from Perkin Elmer Ltd, USA)

**2.2 Synthesis and characterization of CuO and  $^{65}\text{CuO}$  nanoparticles.** CuO nanoparticles were synthesized using a co-precipitation reaction in a water reflux system<sup>14</sup>. 0.511 g of  $\text{CuCl}_2 \cdot 2\text{H}_2\text{O}$  was added to 150 mL of deionized water under stirring conditions followed by addition of 500  $\mu\text{L}$  of glacial acetic acid. The solution was heated to 100°C and under vigorous stirring 0.65 g NaOH was added and left for 10 min. The black precipitate was washed multiple times with deionized water to obtain a phase pure CuO nanoparticles. Isotopically enriched  $^{65}\text{CuO}$  nanoparticles were prepared using the above-mentioned protocol. The isotopic precursors used to synthesize were 99% enriched and procured from Trace Sciences (USA). The concentration of synthesized CuO nanoparticles was measured using Inductively Coupled Plasma-Optical Emission Spectroscopy (ICP-OES, Avio 200, Perkin Elmer, USA) and found to be was 4619 mg/L. Morphology of CuO nanoparticles was investigated with the help of Transmission Electron Microscopy (TEM, FEI 200 KV). The identification of compound along with its phase purity was made by X-Ray

Diffraction analysis (Bruker D8, Cu-K $\alpha$ , 40 kV, 30 mA, 2 $\theta$ =20°-80°). Hydrodynamic size and time dependent suspension stability studies of CuO nanoparticles in DMEM media was performed using Dynamic Light Scattering (Nano ZS, Malvern Instruments, UK) at a concentration of 25 mg/L and at 37°C (pH=7.4).

**2.3 CuO nanoparticles dissolution mediated Elesclomol binding studies.** Dissolution mediated Cu (II) binding to Elesclomol experiments were conducted by taking 25 mg/L of CuO nanoparticles in a dialysis bag (MWCO: 3.5 kDa, Snakeskin, Thermo Fisher) for 24 h in DMEM (Gibco, Invitrogen). Outside the dialysis bag contained 50 mL of phenol red free DMEM and 10  $\mu$ g/mL of Elesclomol (Enzo Life sciences, USA) at 37 °C. By incubating CuO nanoparticles inside the dialysis membrane and suspending the membrane in phenol red free DMEM media, we allowed the passage of copper ions through the dialysis membrane. The changes in the spectral pattern of Elesclomol due to its binding with Cu (II) was recorded with time using UV-Vis measurements (Perkin Elmer UV Vis Lambda 365). Similarly, temporal release of dissolved Cu ions from CuO nanoparticles was measured using ICP-MS analysis (Nexion 2000, Perkin Elmer, USA). The fate of dissolved Cu (II) ions in biological media was assessed by geochemical modelling using MINTEQA2 (Visual MINTEQA2 3.1).

**2.4 Density functional theory (DFT) and molecular dynamics (MD).** The Cu (II)-Elesclomol interactions and binding are modeled using classical molecular dynamics (MD) simulations (GROMACS 5.0.7 software) and density functional theory (DFT) calculations (Gaussian 09 software). To model binding in condensed phase, aqueous solutions of Elesclomol with amino acids were modeled with Cu (II) ions. 50 Elesclomol molecules (double deprotonated), 50 each-



six amino acids (Cys, Ser, Thr, Tyr, Asp<sup>-</sup> and Glu<sup>-</sup>), 50 Cu (II) ions, variable number of Na<sup>+</sup>, Cl<sup>-</sup> ions and ~ 10000 water molecules were used for initial input construction. In the classical MD framework, OPLS-AA force-field parameters<sup>15</sup> for bonded and non-bonded interactions were used, except for the atomic partial charges for columbic interactions, which were derived from the electrostatic potential using DFT calculations. The details for MD simulations, DFT calculations and modified set of the atomic partial charges are provided in the Supporting Information. All classical MD simulations were performed using GROMACS-5.0.7 software package<sup>19</sup>.

For the calculation of charge transfer and theoretical UV-vis spectra, calculations were performed with Gaussian 09, Revision E.01 package<sup>20</sup>. The geometry of Elesclomol and Cu (II)-Elesclomol complexes were optimized using PBE functional<sup>21</sup> with LanL2DZ effective core potential<sup>22</sup> was used for Cu (II) ions and Pople's 6-31+G(d,p) basis was used for other atoms. In case of Cu (II)-Elesclomol complex, deprotonated geometry was used. The details of DFT and TD-DFT calculations are provided in the Supporting Information.

**2.5 Cell viability.** MTT assay was performed to evaluate the mitochondrial activity of A549 cells<sup>23</sup>. 96 well plates were seeded with 5x10<sup>3</sup> cells/well and after 24 h of incubation the cells were treated with a) Elesclomol (1-1000 ng/mL), b) Cu ions (1-20000 ng/mL), c) Cu ions (1-1000 ng/mL) and Elesclomol (50-500 ng/mL), d) CuO nanoparticles (10-20,000 ng/mL), and e) CuO nanoparticles (10-500 ng/mL) and Elesclomol (50 ng/mL). CuCl<sub>2</sub>.2H<sub>2</sub>O was used as the source of Cu (II) ions. 2% H<sub>2</sub>O<sub>2</sub> was used as a positive control and phosphate buffer saline (PBS) was used as negative control. Total and time dependent cell viability was quantified by measuring the absorbance of dissolved formazan product at 590 nm (Biotek, Synergy HT spectrophotometer) and

simultaneously cell morphology was assessed using a phase-contrast microscope for a period of 24 h. The formula used for calculating the cell viability was:

$$\frac{Abs_{590} \text{ sample} - Abs_{590} \text{ medium}}{Abs_{590} \text{ control} - Abs_{590} \text{ medium}} \times 100 \quad \text{Eq 1}$$

**2.6 ROS Assay.** In a time-dependent experiment, the cells (seeding density of  $1.2 \times 10^5$  cells) were exposed to two concentrations of drug (10 and 50 ng/mL), along with three concentrations of CuO Nanoparticles and Cu ions (50, 100, and 200 ng/mL). Post-treatment, the fluorescence intensity was measured using multimode plate reader spectrophotometer (Biotek, Synergy HT spectrophotometer). For intracellular ROS imaging,  $5.0 \times 10^4$  cells were grown on pretreated glass coverslips for 24 h at 37 °C and exposed to 50 ng/mL of Elesclomol, CuO nanoparticles (100 and 200 ng/mL), and a combination of both for 3 h. The cells were rinsed with 1xPBS, treated with 300  $\mu$ L of DCFDA dye (concentration=20  $\mu$ M) and incubated for 30 min at 37 °C. The cells were washed with 1x PBS and the cover slips were mounted on a clean glass slide with prolong gold antifade mounting agent (Thermofisher Scientific) with DAPI and imaged using Confocal Microscope (Leica) and Phase-contrast microscope (Nikon).

**2.7 Annexin V apoptosis assay.** Apoptotic/Necrotic cell population can be recognized by staining cells with Fluorescein Isothiocyanate conjugated (FITC)-Annexin V and Propidium Iodide (PI) dye as per the manufacturer's protocol (BioVision, Milipitas, CA, USA). Briefly, 12 well plates were used to seed  $1.5 \times 10^5$  cells and incubated for 24 h. Cells were then treated with various combination of Elesclomol and CuO nanoparticles for 6 h and 10 h. Afterwards, cells were harvested and washed with PBS, re-suspended in 0.4 mL binding buffer containing 5  $\mu$ L FITC-

Annexin, 5  $\mu$ L PI and incubated for 10 min in dark at room temperature. Cells were analysed using Flow Cytometer (BD FACS Calibur, BD Biosciences, CA).

**2.8 Mitochondrial membrane potential assay.** The effect of CuO nanoparticles with and without Elesclomol on the mitochondrial membrane potential (MMP;  $\Delta\psi$ ) of A549 cells was assessed utilizing cationic dye JC-1 as per the manufacture's protocol (Cayman Chemicals, Ann Arbor, Michigan, USA). Briefly, black clear bottom 96 well plates were used to seed  $1 \times 10^4$  cells and were incubated until reach 80% confluency at 37 °C, 5% CO<sub>2</sub>. After the incubation, the cells were treated with various combination of Elesclomol and CuO nanoparticles for 3 and 6 h. Cells were incubated with 10  $\mu$ L JC-1 dye (dye was diluted in 1:10 ratio in culture medium) for 20 min at 37 °C in dark, 5% CO<sub>2</sub>. Plate was centrifuged for 5 min at 400  $\times$  g and supernatant was discarded. Cells were washed twice with assay buffer. Afterwards, 100  $\mu$ L of assay buffer was added to each well. The mitochondrial membrane potential was represented as the ratio of red:green fluorescence and estimated using multiwell plate reader (BioTek Synergy HT).

**2.9 Live cell imaging.** Live cell imaging were performed to investigate the time dependent ROS generation and changes in cellular behavior on exposure to standalone Elesclomol (50 ng/mL), CuO Nanoparticles (200 ng/mL) and the codelivery of both as compared to the control.  $20 \times 10^3$  were seeded in the glass bottom plates (Nunc, Thermo fisher Scientific) and incubated for 24 h in 37°C, 5% CO<sub>2</sub>. After incubation, the cells were stained with Hoechst and 10  $\mu$ M DCFDA dye in serum free DMEM and were incubated for 30 min. After incubation, the cells were washed with 1x PBS and were exposed to various combination of Elesclomol and CuO nanoparticles and

transferred to live cell imaging setup in confocal microscopy (Leica). Time dependent images were captured for 12 h to observe the ROS generation and changes in the cell morphology.

**2.10 Intracellular trafficking of Cu.** To test the efficacy of Elesclomol drug in transporting Cu (II) ions into the cells, intracellular  $^{65}\text{Cu}$  concentration was measured. In this experiment, 1000 ng/mL of  $^{65}\text{Cu}$  ions ( $^{65}\text{CuCl}_2$  was used as the source of Cu (II) ions), and equivalent  $^{65}\text{CuO}$  were exposed to the cells ( $8.0 \times 10^5$  cells) with and without Elesclomol (50 ng/mL). After incubating for 4 h, the cells were washed with 1x PBS and treated with trypsin for harvesting the cells. The harvested cells were pelletized, freeze-dried and digested using a wet ashing procedure. The ratio of  $\text{HNO}_3:\text{H}_2\text{O}_2$  was 3:1 wherein 4.5 mL  $\text{HNO}_3$  was mixed with 1.5 mL  $\text{H}_2\text{O}_2$  to digest the sample under heating conditions. Calibration curve in the concentration range of 0.00001  $\mu\text{g/mL}$  to 1  $\mu\text{g/mL}$  using  $^{65}\text{Cu}$  ionic standard (99%, 10  $\mu\text{g/mL}$ , Inorganic ventures, USA) was prepared and measured using ICP-MS (Nexion 2000, Perkin Elmer, USA). The measurements were carried out in Helium KED mode<sup>24</sup>.

**2.11 Statistical Analysis.** Biological experiments were done in triplicate ( $n=3$ ), and the data is presented as mean  $\pm$  standard deviation. A student's t-test was performed to obtain the p-value of the independent experimental variable (CuO, Cu ions, Elesclomol groups) compared to the control. The differences were statistically significant at values of  $*p < 0.05$ ,  $**p < 0.01$ ,  $***p < 0.001$ .

### 3. RESULTS AND DISCUSSION

#### 3.1 Characterization of CuO nanoparticles

TEM micrographs of CuO nanoparticles is shown in Figure 2A and the average size for CuO nanoparticles was  $7\pm 1.15$  nm. XRD analysis demonstrates CuO nanoparticles to be phase pure with an average crystallite size of 6.49 nm and having a monoclinic lattice structure (ICDD-PDF 01-073-6023) (Figure 2B). The miller indices (hkl) of the respective XRD peaks are shown in Figure 2B.  $^{65}\text{CuO}$  nanoparticles synthesized in this study were used only for quantifying intracellular accumulation of Cu upon treatment with Elesclomol. For the rest of the studies non-isotopically enriched CuO nanoparticles were used. Characterisation of  $^{65}\text{CuO}$  nanoparticles is shown in Supplementary information (Figure S1, size:  $8.5\pm 1.65$  nm). Suspension stability of CuO nanoparticles was measured by conducting a time dependent hydrodynamic size measurement of CuO nanoparticles in DMEM and deionized water. The analysis showed that the average hydrodynamic size of CuO nanoparticles in deionized water at time  $t= 0.5$  h was 180 nm and reduced to 152 nm after 10 h (Figure 2C). The reduction of hydrodynamic size of CuO nanoparticles is because of sedimentation of bigger particles in deionized water<sup>14, 25, 26</sup>. In case of DMEM (10% FBS), at time  $t=10$  h, the average hydrodynamic size was reduced to 112 nm. Possible reasons for the size reduction are interaction of CuO nanoparticles with ionic species dispersed in DMEM media leading to dissolution<sup>14</sup>. The presence of amino acid, folic acid act as a weak oxidizing agent in the media and facilitates enhanced dissolution of CuO nanoparticles<sup>25</sup>

### **3.2 Dissolution of CuO nanoparticles and Elesclomol-Cu (II) complexation**

Based on CuO dissolution experiment in DMEM media (Figure 3A),  $19.2 \pm 1$  wt% ( $4.8\pm 0.25$  mg/L) of CuO nanoparticles dissolved within 1 h of incubation. Modified first order rate equation was used to perform the best fit of the dissolution profile at different time points and to calculate the rate of dissolution<sup>13</sup>. The dissolution rate ( $k=1.39$  h<sup>-1</sup>) was high with almost  $82.6\pm 1$  wt%

( $20.5 \pm 0.50$  mg/L) of the nanoparticles dissolving in the first 4 h and saturating to  $85.2 \pm 3.6$  wt% ( $21.3 \pm 0.9$  mg/L) by 24 h of incubation. UV-Vis spectroscopy analysis was performed in order to demonstrate Elesclomol-binding with copper ions. The Elesclomol suspended in the DMEM was available for complexation with the dissolved and released Cu (II) ions. Figure 3B shows the UV-Vis spectrum of Elesclomol drug as a control ( $10 \mu\text{g/mL}$ ), with maximum absorbance at 279 nm. After 1 h of dissolution of CuO nanoparticles, there was a significant decrease in the peak intensity at 279 nm, indicating the binding of Elesclomol with copper ions (Figure 3B). On increasing the time, there was a gradual change in the main peak of Elesclomol at 279 nm and a concomitant emergence of an absorption peak at 360 nm (due to the spontaneous formation of Cu-Elesclomol complexes). Since, there is a significant generation of Cu ions from the CuO nanoparticles, the Cu (II) ions binds to Elesclomol molecule at 1:1 molar ratio and starts to precipitate<sup>8</sup>. It is the reason why the characteristic peak of Elesclomol starts shifting and becomes flattened later when all Elesclomol molecule formed complex with free Cu (II) ions. The formation of Cu-Elesclomol complex can be observed from its characteristic peak at 365 nm. Since, the medium is aqueous and the complex is electrophoretically neutral, the Cu (II)-Elesclomol complex precipitates and the peak at 365 nm was not observed after 4 h. However, this complex formation and precipitation did not show any impact in the bioavailability of Cu (II)-Elesclomol complex to A549 cells as demonstrated through ROS assay and cell viability assay. It is because, once the free Elesclomol molecule forms complex with Cu (II) ions, the structure of the Elesclomol molecules changes from distorted to planar (Figure 4A,4B), which facilitates active uptake of the Elesclomol-Cu (II) complex inside the cells<sup>8</sup>. The Elesclomol in DMEM ( $10 \mu\text{g/mL}$ ) was found to be stable for a period of 4 h (Figure S2). The slight reduction in peak intensity of Elesclomol can be because of unwanted complexation of Elesclomol with other divalent metal ions present in media.

### 3.3 Validation of Elesclomol-Cu (II) binding using MD and DFT studies

To investigate the extent of free Cu (II) ions available to bind with Elesclomol, geochemical modelling using MINTEQ software was performed for copper salt in biologically relevant media (viz. simulated body fluid and artificial lysosomal fluid). The modelling data showed that in more complex biological media, the availability of free Cu (II) ions reduced significantly as it readily forms complex with the various organic/inorganic molecule. For example, in artificial lysosomal fluid, 98% of Cu (II) ions are present in Cu-organic complexes with <1% Cu (II) ions exists in Free State. Similarly, in case of simulated body fluid, the MINTEQ analysis showed that 36% of Cu (II) ions are present in Cu-organic complexes, 54% Cu-inorganic complexes and remaining 10% as Cu (I) and Cu (II) ions<sup>14</sup>. Therefore, condensed phase model was simulated using classical OPLS-AA force-field<sup>15</sup> to understand the competitive behavior of Cu (II) ion binding with Elesclomol/amino acids present in the biological fluids. 50 molecules of each amino acid in water (1:100 molecular ratios) were simulated first to prepare and benchmark individual amino acid solutions. 50 molecules of each amino acid along with 50 Elesclomol molecules were equilibrated in a box of the side of 10 nm. 50 Cu (II), Na<sup>+</sup> and Cl<sup>-</sup> ions, and ~ 10000 water molecules were used to solvate the mixture thoroughly. After equilibration at T = 350 K under isothermal-isobaric ensemble, the system was cooled down to T = 300 K for the final production run (Figure 4E, 4F). Radial distribution of more negatively charged atoms – carboxylate groups of Asp<sup>-</sup> and Glu<sup>-</sup>, and C=S, C=O, N<sup>-</sup> of deprotonated Elesclomol molecules around Cu (II) ions were calculated (Figure 4G). The computed RDF suggests C=O (Elesclomol) to be the most strongly interacting site with Cu (II) ions. While Asp<sup>-</sup> has a slightly higher coordination with Cu (II) ions, presence of three type

of sites (C=O, C=S, N<sup>-</sup>, total six on each Elesclomol molecule) suggest Elesclomol to be the preferred host for Cu (II) ions (Figure 4H).

The results from classical simulation, also led to examination of local geometries. In addition to already known tetradentate N<sup>-</sup>, N<sup>-</sup>, S, S coordinated geometry, GM1, proposed by Wu et al.<sup>16</sup> (Figure 4A), another geometry was also discovered during various potential energy scans of Cu (II) with doubly deprotonated Elesclomol (Figure 4B). The new geometry (N<sup>-</sup>, O, S, S coordinated), GM2, is slightly higher in energy than the other. This geometry could be the initial key configuration which forms first and later transforms to the more stable configuration (Figure 4A). In addition to the geometrical information, Figure S3 also shows the distribution of atomic partial charges in the local geometries calculated using CHELPG method<sup>17</sup>. It suggests a net charge transfer from Cu (II) to Elesclomol<sup>2-</sup> to be 1.365 e<sup>-</sup> for GM1 and 1.240 e<sup>-</sup> for GM2. The electrostatic potential is mapped on the surface of electron density to exhibit the charge distribution in the geometries (Figure 4C, 4D). To validate the hypothesis that the decrease in 279 nm peak and emergence of 360 nm plateau could be a signature of Cu (II)-Elesclomol binding, TDDFT calculations were performed using PBE/LanL2DZ & 6-31+G(d,p) method (details are provided in the Supporting Information) to calculate theoretical UV-vis spectra for Elesclomol and Cu (II)-Elesclomol complex (GM1 geometry). The calculated spectra (Figure 3C) suggests that for Elesclomol, the highest intensity peak appears at 275 nm, and for Cu (II)-Elesclomol complex, at 380 nm. Thus, the calculated spectra from TDDFT not only produces a close agreement with experimental values (Figure 3B) but also validates the hypothesis of plateau at 360 nm in experimental spectra to be a peak corresponding to Cu (II)-Elesclomol complex.

### **3.4 Co-delivery of CuO nanoparticles and Elesclomol: Cell viability**



Cell viability of A549 (Pulmonary Adenocarcinoma) cells was studied after the exposure of i) Elesclomol, ii) CuO nanoparticles, iii) Cu (II) ions, iv) Elesclomol and Cu (II) ions, and v) Elesclomol and CuO nanoparticles (Figure 5 A-C). Elesclomol alone showed a negligible impact on viability of A549 cells, wherein 90% of the cells were viable at 50 ng/mL of Elesclomol after 24 h (Figure 5A). The positive control (2% H<sub>2</sub>O<sub>2</sub>) showed >95% reduction in the cell viability after 24 h exposure. The cell viability decreased to ~30% and ~40% at 100 and 1000 ng/mL of Elesclomol exposure, respectively. Figure 5A shows that the exposure of lower concentrations of CuO nanoparticles (10-500 ng/mL) leads to >80% of A549 cells viability. However, the cell viability was found to be reduced to 22% and 40% at 1000 ng/mL and 10µg/mL of CuO nanoparticle exposure (Figure S8). In case of Cu ions, the cell viability was reduced by 15% and 35% when exposed to 1 µg/mL and 20 µg/mL of Cu ions, respectively (Figure S8). In cancer nanomedicine, the dosage or exposure concentration of nanoparticles is extremely critical component. The CuO nanoparticles are toxic to mammalian cells at a higher exposure concentration. Ahamed et al (2010) reported that the standalone CuO nanoparticles are toxic to A549 cells in a dose dependent manner by induction of lipid peroxidation, glutathione depletion, induction of superoxide dismutase etc. The cytotoxicity assay showed that at the exposure concentration of 10, 25, 50 µg/ml CuO nanoparticles, the reduction in cell viability was observed to be 25%, 34%, and 52% respectively<sup>38</sup>. However, at lower concentration i.e., <10 µg/ml, the CuO nanoparticles aren't significantly toxic to the mammalian cells and goes in agreement with the cytotoxicity data reported in Figure S8. The exposure concentration of CuO nanoparticles used in our study was < 0.5 µg/ml and at such a low exposure concentration, it is unlikely to have any harmful impact on the mammalian cells.

In a separate experiment, Elesclomol drug (10-500 ng/mL) was exposed to A549 cells in presence of Cu ions (1 ng/mL to 5000 ng/mL) (Figure 5B). After 24 h of incubation, there was a significant ( $***p < 0.001$ ) decrease in cell viability after the exposure of increased Cu (II) ions concentration. We selected the Elesclomol concentration of 50 ng/mL for all our further experiments because (i) Elesclomol has a high affinity to bind with Cu (II) ions even at lower concentrations, (ii) significant reduction in cellular viability at 50 ng/mL of Elesclomol concentration, and (iii) reducing the Elesclomol quantity and hence making it cost effective. Figure 5C shows a comparison of A549 cell viability on exposure of Cu ions, CuO nanoparticles, Elesclomol + Cu ions, and Elesclomol + CuO nanoparticles. After 24 h of exposure of CuO nanoparticles and Elesclomol, an exposure of 50 ng/mL of nanoparticles and 50 ng/mL of Elesclomol was enough to reduce the viability of A549 cells by 50%. Similarly, at a high exposure concentration of 250 ng/mL and 500 ng/mL of CuO nanoparticles, almost 90% of the cells were found to be dead. Interestingly, when CuO nanoparticles and 50 ng/mL of Elesclomol were exposed together to A549 cells, there was a significant ( $***p < 0.001$ ) reduction in cell viability compared to all other combinations. For example,  $85 \pm 4\%$  of cell viability when exposed to 50 ng/mL of Elesclomol,  $83 \pm 5\%$  viability when exposed to 50 ng/mL of CuO nanoparticles, and  $52 \pm 8\%$  viability when exposed to 50 ng/mL of Elesclomol and 50 ng/mL of CuO nanoparticles. Figure 5D represents a time-dependent (up to 24 h) A549 cell toxicity profile of A549 cells when exposed to a) 50 ng/mL of Elesclomol, b) 500 ng/mL of CuO nanoparticles, and c) co-delivery of 500 ng/mL CuO nanoparticles and 50 ng/mL of Elesclomol. Only Elesclomol did not have any significant toxicity to the A549 cells (Figure 5D). For CuO nanoparticles, the cell viability was  $78 \pm 3\%$  at the end of 24 h. However, in case of co-delivery of CuO nanoparticles with Elesclomol, the cell viability was reduced to  $8.5 \pm 2\%$  after 24 h. In case of CuO nanoparticles and Elesclomol co-delivery, the cell viability reduced rapidly

within 1 h of exposure, i.e.  $86\pm 2\%$  in 0.25 h,  $74\pm 3\%$  in 0.5 h, and  $71\pm 4\%$  in 1 h. Microscopic imaging performed at 6 h, showed the A549 cells to become spherical-shaped, which could be due to the loss of cell membrane integrity and approaching to apoptosis (Figure 5E and Figure S4). At 8 and 12 h, majority of the cells underwent apoptosis, which is also in accordance with the time-dependent cytotoxic profile of A549 cells. Microscopic analysis showed that co-delivery of Elesclomol and CuO nanoparticles for 4 h could induce a significant impact on the cell morphology compared to the exposure of Elesclomol and CuO nanoparticles individually (Figure S5). On increasing the Elesclomol concentration from 10 - 100 ng/mL, more cells were found approaching apoptosis.

### **3.5 Co-delivery of Elesclomol and CuO nanoparticles: Enhanced oxidative stress**

Results from Figure 5D demonstrates that the cell viability starts reducing rapidly after the end of 3 h of CuO nanoparticles and Elesclomol exposure. Therefore, ROS production in A549 cells on exposure to 10 ng/mL of Elesclomol with three different concentration of copper ions and CuO nanoparticles (50, 100 and 200 ng/mL) was followed from 1-4 h (Figure 6A and 6B). The reason of selecting 10 ng/mL of Elesclomol was to demonstrate if the drug is still efficient to generate ROS at concentration lesser than 50 ng/mL. The fold change in ROS generation was not significant when the cells were exposed to copper ions or Elesclomol, alone. For a combination of 10 ng/mL of Elesclomol and 200 ng/mL of Cu ions, exposed for 4 h, there was a 1.1-fold increase in ROS production. In contrast, there was a significant increase in ROS, such as 1.83-fold (10 ng/mL Elesclomol+50 ng/mL CuO nanoparticles), 2.3-fold (10 ng/mL Elesclomol+100 ng/mL CuO nanoparticles), and 2.5-fold (10 ng/mL Elesclomol+ 200 ng/mL CuO nanoparticles). ROS production did not necessarily increase by increasing the Cu (II) concentration or the Elesclomol

concentration. However, in case of Elesclomol + CuO nanoparticles exposure, there was a ~180% increase for 50 ng/mL Elesclomol + 50 ng/mL CuO nanoparticles, ~190% increase for 50 ng/mL Elesclomol + 100 ng/mL CuO nanoparticles, and ~330% increase for 50 ng/mL Elesclomol + 200 ng/mL CuO nanoparticles.

Figure 7 (A-C) shows the CLSM images representing the time-dependent ROS production by A549 cells. At 1 h, the untreated control cell showed a minimal ROS production and some dead cells. As compared to standalone treatment of CuO (100 ng/mL) nanoparticles and Elesclomol (50 ng/mL), very high ROS production was recorded when Elesclomol and CuO nanoparticles were co-delivered at equivalent concentration. Similarly, the ROS production significantly increased after 2 h of exposure as compared to the control cells. 50 ng/mL of Elesclomol co-delivered with 100 ng/mL and 200 ng/mL of CuO nanoparticles showed a very high ROS production after the exposure time of 2 h (Figure 7B). However, the fluorescent intensity of DCFDA dye was reduced significantly after the end of 3 h, and there was an increase in blue emission suggesting the uptake of DAPI by dead cells (Figure 7C and Figure S6). To appropriately quantify or image ROS production, the cells are required to be attached to the surface of the plate and therefore all our ROS quantification were performed for the first 4 h. Although, co-delivery of 10 ng/mL Elesclomol drug + CuO nanoparticles were not showing a significant impact on the cell morphology (Figure S4), ROS measurements (Figure 6B) demonstrated that 10 ng/mL Elesclomol exposure to have substantial ROS generation after the end of 4 h.

Live cell imaging experiments were also performed to validate the intracellular ROS mediated cellular death. For untreated cells used as control the cells were healthy until the end of the experiment (12 h) with no significant abnormality observed. In case of standalone exposure of Elesclomol (50 ng/mL) and CuO nanoparticles (200 ng/mL), majority of the cells were healthy but

there were few cell deaths observed after the end of 8 h. However, the co-delivery of Elesclomol (50 ng/mL) and CuO nanoparticles (200 ng/mL) demonstrated a high ROS generation, which can be observed through development of green fluorescence from the cells. The initial ROS generation (up to 3 h) goes in agreement with the ROS assay findings from flow cytometry and fluorescent spectroscopy analysis. It was also observed that most of the cells are undergoing apoptosis after the end of 8 h of experiment. The live cell videos are attached in the Supplementary information file (Supplementary video files control.mp4, Elesclomol+CuO.mp4, only CuO treated.mp4, only Elesclomol treated.mp4). A time dependent production of ROS and changes in cell morphology in live cell imaging has been shown in Figure 7D and Figure S7. In Figure 7D, the 8<sup>th</sup> h image marked with black arrow shows the cells are undergoing apoptosis in case of co-delivery of Elesclomol (50 ng/mL) and CuO nanoparticles (200 ng/mL) due to enhanced ROS production as demonstrated in initial time points.

### **3.6 Mitochondrial membrane depolarization**

Loss in mitochondrial membrane potential is a key indicator for apoptosis and can be utilized to discriminate between healthy and apoptotic cells. We estimated the fold change in red to green fluorescence ratio with respect to control untreated cells. The red:green fluorescence ratio of JC-1 dye decreases with elevation in mitochondrial depolarization. As evident, from Figure 8A that Elesclomol and 100 ng/mL CuO nanoparticles show negligible changes in the red to green fluorescence ratio as compared to control suggesting that it did not remarkably alter mitochondrial function. However, increasing concentration of CuO nanoparticles (200 ng/mL) displayed gradient decrease in red/green fluorescence ratio after 6 h treatment and was less than ~0.7 fold suggesting mitochondrial depolarization. Interestingly, Elesclomol co-delivered with CuO nanoparticles (100

ng/mL) caused ~0.65-fold change in red to green fluorescence ratio after 3 and 6 h treatments. Further, 6 h treatment of Elesclomol co-delivered with 200 ng/mL CuO nanoparticles showed more pronounced effect causing ~0.5-fold decrease in red to green fluorescence. Overall, the results suggested that 6 h exposure of Elesclomol co-delivered with CuO nanoparticles enhances the depolarization of mitochondrial membrane potential. The mitochondrial membrane depolarisation initiates a cascade of events leading to the cellular apoptosis.

### **3.7 Elesclomol facilitating high intracellular Cu trafficking**

To establish that CuO nanoparticles acts as a reservoir for the slow and sustained release of copper ions to be ferried into the cell to be true, we quantified the intracellular total copper for A549 cells after exposure to stable isotope enriched  $^{65}\text{CuO}$  nanoparticles and Elesclomol treatment. The stable isotope-labeled nanoparticles tracing takes place against the natural background and majorly reliant on measuring the isotopic changes in the biological cells that result from the exposure of nanoparticles synthesized using enriched isotopic constituent. 100%  $^{65}\text{Cu}$  enriched  $^{65}\text{CuO}$  nanoparticles were synthesized, with similar physicochemical properties to non-isotopically labelled CuO nanoparticles. The background concentration of  $^{65}\text{Cu}$  was measured to be  $19.37 \pm 3.2$  ng/mL in A549 cells. The A549 cells were exposed with 1000 ng/mL of  $^{65}\text{Cu}$  ions and 1000 ng/mL of  $^{65}\text{CuO}$  nanoparticles with and without 50 ng/mL of Elesclomol. After 3 h of incubation without Elesclomol (Figure 8B), the total cellular concentration of  $^{65}\text{Cu}$  was found to be  $120.5 \pm 4.8$  ng/mL when ionic tracer was used (i.e.,  $^{65}\text{Cu}$  ions); whereas for  $^{65}\text{CuO}$  nanoparticles, the accumulation of  $^{65}\text{Cu}$  inside the cells was measured as  $184.05 \pm 7.6$  ng/mL. The reason of increase in cellular concentration of  $^{65}\text{Cu}$  ions from  $^{65}\text{CuO}$  nanoparticles exposure can be because of internalization and accumulation of  $^{65}\text{CuO}$  nanoparticles itself into the cells. In the presence of 50 ng/mL of

Elesclomol, the concentration of  $^{65}\text{Cu}$  increased in the cells increased significantly for both  $^{65}\text{Cu}$  ions and  $^{65}\text{CuO}$  nanoparticles. The measured concentration of  $^{65}\text{Cu}$  was  $544 \pm 10.4$  ng/mL and  $847 \pm 11$  ng/mL for  $^{65}\text{Cu}$  ionic exposure and  $^{65}\text{CuO}$  nanoparticulate exposure. According to the dissolution profile of CuO in DMEM (10% FBS) media,  $71.4 \pm 2$  wt% of CuO gets dissolved within 3 h of its exposure to media. It signifies that more extracellular copper ions were available to Elesclomol molecules from dissolution of  $^{65}\text{CuO}$  nanoparticles to transport inside the cells as compared to standalone exposure of  $^{65}\text{Cu}$  ions. On investigating the amount of  $^{65}\text{Cu}$  ions remaining in the media, it was found that  $390 \pm 4$  ng/mL from only  $^{65}\text{Cu}$  ions samples and  $133.4 \pm 6$  ng/mL from  $^{65}\text{CuO}$  samples were still present in the samples either in the form of  $^{65}\text{Cu}$  complexes or undissolved  $^{65}\text{CuO}$  nanoparticles.

### **3.8 Cancer cells undergoing apoptosis on exposure to CuO and Elesclomol**

An important hallmark for apoptosis is externalization of phosphatidylserine to the outer leaflet of the cell membrane, which can be experimentally quantified by the annexin V binding. Annexin V/PI double positive cells signify the apoptotic cell population. Likewise, 6 h exposure of Elesclomol (50 ng/mL) co-delivered with CuO nanoparticles (500 ng/mL) demonstrated the increase in apoptotic cell population  $\sim 11.45\%$  with most of the cells in late apoptotic stage (Annexin-V/PI double positive, Figure 9). However, 10 h treatment showed a drastic increase in apoptotic cells population  $\sim 22.80\%$  for Elesclomol (50 ng/mL) co-delivered with CuO nanoparticles (200 ng/mL) and  $\sim 69.90\%$  Elesclomol (50 ng/mL) co-delivered with CuO nanoparticles (500 ng/mL). The data goes in agreement with the live cell imaging (Figure 7D), cytotoxicity assays (Figure 5) that shows there was an enhanced ROS production until 3-4 h of the CuO and Elesclomol exposure and later the cells are undergoing apoptosis after the 6-8 h.

### 3.9 Proposed Mechanism for enhanced oxidative stress generation

Elesclomol drug is known to preferentially bind with copper ions and act as a shuttle to transport Cu ions inside the cells and, more specifically to mitochondria<sup>7</sup>. The proposed mechanism of enhanced ROS generation is shown in Figure 1. Briefly, once inside the cell, the major cause of cellular toxicity of Cu (II) ions is due to the generation of reactive oxygen species. The shuttling of Cu (II) ions by Elesclomol is a spontaneous process wherein once the Cu (II) ions are delivered inside the mitochondria by the drug molecule; due to a reducing environment in mitochondria, the Cu (II) in the Cu (II)-Elesclomol complex gains one electron and reduces to Cu (I). Once the reduction happens, the Cu (I) gets out of the complex and creates an alteration in the electron transport chain and generates ROS by Fenton-like reaction. The free Elesclomol gets effluxed out of the cells to complex with other free Cu (II) ions present outside the cell and repeat the entire shuttling process<sup>7</sup>. The presence of Cu (I) ions becomes the source of generation hydroxyl radicals (OH·) due to Fenton reaction<sup>36</sup>. As shown in Figure 1, Cuprous ions reacts with mitochondrial hydrogen peroxide and build up high concentration of hydroxyl radical inside the cells. These hydroxyl radicals. The excess buildup of ROS inside the cells can induce damages to lipids, proteins, nucleic acids and organelles and further lead to apoptosis through the activation of caspase pathways<sup>37</sup>.

Therefore, the observations from Figure 5B suggest that it is important that free Cu (II) ions must be available at extracellular milieu so that the drug can make an active complex with Cu(II) ions. However, in a complex cell culture media such as DMEM, there are various other Cu complex-forming agents such as ascorbate, glutamic acid, folic acid, etc. that can quickly form complex with Cu (II) and reduce the number of free available Cu (II) ions to form complex with Elesclomol causing lower amount of Cu (II) ions to be transported inside the cells and generate oxidative



stress. The molecular dynamic and DFT based studies suggested that even in presence of Cu-complex forming agents like amino acids; dissolved Cu (II) ions generated from dissolution of CuO nanoparticles preferentially binds to Elesclomol. This will help in increased Elesclomol mediated transportation of Cu (II) through redox chemistry and induce lethal oxidative stress. This enhanced toxicity towards A549 cells could be explained by the dissolution profile of CuO nanoparticles (Figure 3A).  $85.2 \pm 3.6$  wt% of CuO nanoparticles dissolves after 24 h. It also demonstrated that significant amount of dissolved Cu(II) ions are already available for Elesclomol to be transported inside the mitochondria and generate enhanced oxidative stress. The CuO nanoparticles act as a reservoir from which a gradual release of copper ions happens and thus allowing Elesclomol to bind and shuttle Cu (II) inside the cell. In comparison, Cu (II) ions easily form complexes as soon as it is exposed to cell culture media, which reduces the Cu (II)-Elesclomol complexation and its intracellular trafficking. Due to the shuttling mechanism of the Elesclomol, the free Cu (II) ions availability becomes the limiting factor because the majority of Cu (II) ions forms complexes with various complex-forming agents. However, in case of CuO nanoparticles, the slow and sustained release of Cu ions allows a time lag for free Elesclomol molecules to complex with available free Cu (II) and transports it inside the mitochondria. The dissolution of CuO nanoparticles, therefore, provides a constant supply of Cu (II) ions for a longer duration to Elesclomol and hence makes it a better candidate for inducing prolonged oxidative stress. According to Du et al (2020)<sup>35</sup>, there is a positive correlation between the ROS production with that of dissociation constant (pKa) of an organic compound. The reported theoretically calculated pKa value of 11.41 for Elesclomol-Cu(II) complex, is considered to be higher in the reducing environment like mitochondria. We expect a significant difference in the antitumor activity *in vivo* because of various other underlying reasons (e.g., Enhanced Permeation and

Retention effect, rapid angiogenesis)<sup>18</sup>. The parameters like the EPR effect and rapid angiogenesis are not present in normal cells. Since, the tumor cells have elevated ROS level as compared to normal cells, the enhanced oxidative stress increases the ROS level and exhaust the antioxidant capacity of the tumor, resulting in apoptotic pathways. The cancer cells operate with higher ROS level with reduced anti-oxidant capacity than normal cells. These unique features make cancer cells more vulnerable to Elesclomol-Cu (II) complexes that enhances the oxidative stress.

#### **4. CONCLUSIONS**

In our study, CuO nanoparticles were found to act as a reservoir of copper ions facilitating slow and controlled dissolution in the cell culture media offering a sustained and steady supply of copper ions for Elesclomol to bind. Cytotoxicity and ROS experiments demonstrated the percentage of cell death and ROS generation were very high during the initial time and was sustained after that. The generated dissolved species allowed the Elesclomol molecules to shuttle these dissolved Cu ions inside the mitochondria to produce ROS mediated cell death. The activity of the Cu-Elesclomol complex was rapid, with approximately 80% of the cell death occurring within 12 h. It was shown that 50 ng/mL Elesclomol when co-delivered with CuO nanoparticles at the concentration from 50-100 ng/mL is enough to reduce the cell viability by >50%. As demonstrated through ROS quantification and live cell imaging, the ROS production in A549 cells are at its peak at 3-4 h after the exposure of 50 ng/mL Elesclomol and 100 ng/mL CuO nanoparticles. Through live cell imaging and ROS quantification, it was observed that the cells were generating high ROS upto 3-4 h, loss of membrane integrity at 4 to 6 h and undergoing apoptosis after 6 h. The dissolved ions from CuO nanoparticles readily formed a complex with Elesclomol drug and were transported to mitochondria to generate intracellular ROS. The theoretical values provide support to the correct

assignment of 360 nm plateau region observed in experimental spectra, due to formation of Cu (II)-Elesclomol complex. The stable isotope labeling approach helped in demonstrating a high amount of Cu ions being trafficked inside the cells. It also demonstrated that only extracellular Cu ions being trafficked inside the cells through the shuttling mechanism of Elesclomol drug. The co-delivery approach minimized the Elesclomol dosage requirement (50 ng/mL) compared to some of the other anticancer drugs commonly used as anticancer agents. The nanoparticle enabled co-delivery route showed a promising approach towards the toxicity of cancer cells through CuO nanoparticle dissolution mediated oxidative stress based anticancer therapy.

## **ASSOCIATED CONTENT**

Supporting Information:

Data from published literature on efficacy of Elesclomol; characterization of <sup>65</sup>CuO nanoparticles; time dependent stability of Elesclomol in DMEM; DFT methodology and data set; cell morphology and ROS imaging data set.

Control (.mp4), Elesclomol+CuO (.mp4), Only CuO treated (.mp4), only Elesclomol treated (.mp4) file for live cell imaging of ROS production.

## **AUTHOR INFORMATION**

### **Corresponding Author**

\*Dr. Swaroop Chakraborty ([s.chakraborty@bham.ac.uk](mailto:s.chakraborty@bham.ac.uk)); ORCID Id- 0000-0002-4388-4964

\*Dr. Superb Misra ([smisra@iitgn.ac.in](mailto:smisra@iitgn.ac.in)) ORCID Id- 0000-0001-5551-2706

### **Author Contributions**

**SC:** Conceptualization, Methodology, Validation, Investigation, Formal analysis, Writing, Visualization, Editing. **PP-** Investigation, Formal analysis, Writing, **JS:** Investigation, Formal Analysis, Writing. **CM:** Investigation **RR:** Conceptualization, **VS:** Conceptualization, Editing. **SS:** Visualization, Editing. **EVJ:** Visualization, Editing **SM:** Conceptualization, Visualization, Editing

### **Funding Sources**

This work has been financially supported by IMPRINT (Project No. 6408, MHRD), and SERB-CRG (CRG/2019/006165). VS acknowledges funding through DBT (Grant nos. BT/PR15214/BRB/10/1449/2015 and BT/RLF/re-entry/45/2015) and DST-SERB (grant no. ECR/2016/000913).

### **ACKNOWLEDGMENT**

We acknowledge Dr. Dhiraj Bhatia's (Assistant Professor, IIT Gandhinagar) support with live cell imaging of the samples. We also acknowledge Chantal Jackson (University of Birmingham, UK) to support us with formatting the figures used in the manuscript.

### **REFERENCES**

- (1) Angelé-Martínez, C.; Nguyen, K. V. T.; Ameer, F. S.; Anker, J. N.; Brumaghim, J. L. Reactive Oxygen Species Generation by Copper(II) Oxide Nanoparticles Determined by DNA Damage Assays and EPR Spectroscopy. *Nanotoxicology* 2017, 11 (2). <https://doi.org/10.1080/17435390.2017.1293750>.
- (2) Vinardell, M. P.; Mitjans, M. Antitumor Activities of Metal Oxide Nanoparticles. *Nanomaterials*. 2015. <https://doi.org/10.3390/nano5021004>.

- (3) Postovit, L.; Widmann, C.; Huang, P.; Gibson, S. B. Harnessing Oxidative Stress as an Innovative Target for Cancer Therapy. *Oxidative Medicine and Cellular Longevity*. 2018. <https://doi.org/10.1155/2018/6135739>.
- (4) Din, F. U.; Aman, W.; Ullah, I.; Qureshi, O. S.; Mustapha, O.; Shafique, S.; Zeb, A. Effective Use of Nanocarriers as Drug Delivery Systems for the Treatment of Selected Tumors. *International Journal of Nanomedicine*. 2017, pp 7291–7309. <https://doi.org/10.2147/IJN.S146315>.
- (5) Jabir, N. R.; Tabrez, S.; Ashraf, G. M.; Shakil, S.; Damanhour, G. A.; Kamal, M. A. Nanotechnology-Based Approaches in Anticancer Research. *International Journal of Nanomedicine*. 2012, pp 4391–4408. <https://doi.org/10.2147/IJN.S33838>.
- (6) Kirshner, J. R.; He, S.; Balasubramanyam, V.; Kepros, J.; Yang, C. Y.; Zhang, M.; Du, Z.; Barsoum, J.; Bertin, J. Elesclomol Induces Cancer Cell Apoptosis through Oxidative Stress. *Mol. Cancer Ther.* 2008, 7 (8), 2319–2327. <https://doi.org/10.1158/1535-7163.MCT-08-0298>.
- (7) Nagai, M.; Vo, N. H.; Ogawa, L. S.; Chimmanamada, D.; Inoue, T.; Chu, J.; Beaudette-Zlatanova, B. C.; Lu, R.; Blackman, R. K.; Barsoum, J.; Koya, K.; Wada, Y. The Oncology Drug Elesclomol Selectively Transports Copper to the Mitochondria to Induce Oxidative Stress in Cancer Cells. *Free Radic. Biol. Med.* 2012, 52 (10), 2142–2150. <https://doi.org/10.1016/j.freeradbiomed.2012.03.017>.
- (8) Yadav, A. A.; Patel, D.; Wu, X.; Hasinoff, B. B. Molecular Mechanisms of the Biological Activity of the Anticancer Drug Elesclomol and Its Complexes with Cu(II), Ni(II) and Pt(II). *J. Inorg. Biochem.* 2013, 126, 1–6. <https://doi.org/10.1016/j.jinorgbio.2013.04.013>.

- (9) Carloni, P.; Rothlisberger, U.; Parrinello, M. The Role and Perspective of Ab Initio Molecular Dynamics in the Study of Biological Systems. *Acc. Chem. Res.* 2002, 35 (6), 455–464. <https://doi.org/10.1021/ar010018u>.
- (10) De Vivo, M.; Masetti, M.; Bottegoni, G.; Cavalli, A. Role of Molecular Dynamics and Related Methods in Drug Discovery. *Journal of Medicinal Chemistry*. 2016, pp 4035–4061. <https://doi.org/10.1021/acs.jmedchem.5b01684>.
- (11) Tidjani-Rahmouni, N.; Bensiradj, N. E. H.; Djebbar, S.; Benali-Baitich, O. Synthesis, Characterization, Electrochemical Studies and DFT Calculations of Amino Acids Ternary Complexes of Copper (II) with Isonitrosoacetophenone. *Biological Activities. J. Mol. Struct.* 2014, 1075, 254–263. <https://doi.org/10.1016/j.molstruc.2014.06.067>.
- (12) Wu, Z.; Fernandez-Lima, F. A.; Russell, D. H. Amino Acid Influence on Copper Binding to Peptides: Cysteine versus Arginine. *J. Am. Soc. Mass Spectrom.* 2010, 21 (4), 522–533. <https://doi.org/10.1016/j.jasms.2009.12.020>.
- (13) Utembe, W.; Potgieter, K.; Stefaniak, A. B.; Gulumian, M. Dissolution and Biodurability: Important Parameters Needed for Risk Assessment of Nanomaterials. *Particle and Fibre Toxicology*. 2015. <https://doi.org/10.1186/s12989-015-0088-2>.
- (14) Chakraborty, S.; Nair, A.; Paliwal, M.; Dybowska, A.; Misra, S. K. Exposure Media a Critical Factor for Controlling Dissolution of CuO Nanoparticles. *J. Nanoparticle Res.* 2018, 20 (12). <https://doi.org/10.1007/s11051-018-4428-7>.

(15) Jorgensen, W. L.; Maxwell, D. S.; Tirado-Rives, J. Development and Testing of the OPLS All-Atom Force Field on Conformational Energetics and Properties of Organic Liquids. *J. Am. Chem. Soc.* 1996, 118 (45), 11225–11236. <https://doi.org/10.1021/ja9621760>.


(16) Wu, L.; Zhou, L.; Liu, D. Q.; Vogt, F. G.; Kord, A. S. LC-MS/MS and Density Functional Theory Study of Copper(II) and Nickel(II) Chelating Complexes of Elesclomol (a Novel Anticancer Agent). *J. Pharm. Biomed. Anal.* 2011, 54 (2). <https://doi.org/10.1016/j.jpba.2010.09.007>.

(17) Spackman, M. A. Potential Derived Charges Using a Geodesic Point Selection Scheme. *J. Comput. Chem.* 1996, 17 (1), 1–18. [https://doi.org/10.1002/\(SICI\)1096-987X\(19960115\)17:1<1::AID-JCC1>3.0.CO;2-V](https://doi.org/10.1002/(SICI)1096-987X(19960115)17:1<1::AID-JCC1>3.0.CO;2-V).

(18) Shah, M. R.; Imran, M.; Ullah, S. Nanocarrier-Based Targeted Pulmonary Delivery: Novel Approaches for Effective Lung Cancer Treatment. In *Nanocarriers for Cancer Diagnosis and Targeted Chemotherapy*; 2019; pp 129–161. <https://doi.org/10.1016/b978-0-12-816773-1.00006-7>.

(19) Abraham, M. J.; Murtola, T.; Schulz, R.; Páll, S.; Smith, J. C.; Hess, B.; Lindah, E. Gromacs: High Performance Molecular Simulations through Multi-Level Parallelism from Laptops to Supercomputers. *SoftwareX* 2015, 1–2, 19–25. <https://doi.org/10.1016/j.softx.2015.06.001>.

(20) Frisch, M. J.; Trucks, G. W.; Schlegel, H. B.; Scuseria, G. E.; Robb, M. A.; Cheeseman, J. R.; Scalmani, G.; Barone, V.; Mennucci, B.; Petersson, G. A.; Nakatsuji, H.; Caricato, M.; Li, X.; Hratchian, H. P.; Izmaylov, A. F.; Bloino, J.; Zheng, G.; Sonnenberg, J. L.; Hada, M.; Ehara, M.;

Toyota, K.; Fukuda, R.; Hasegawa, J.; Ishida, M.; Nakajima, T.; Honda, Y.; Kitao, O.; Nakai, H.; Vreven, T.; Montgomery Jr., J. A.; Peralta, J. E.; Ogliaro, F.; Bearpark, M.; Heyd, J. J.; Brothers, E.; Kudin, K. N.; Staroverov, V. N.; Kobayashi, R.; Normand, J.; Raghavachari, K.; Rendell, A.; Burant, J. C.; Iyengar, S. S.; Tomasi, J.; Cossi, M.; Rega, N.; Millam, J. M.; Klene, M.; Knox, J. E.; Cross, J. B.; Bakken, V.; Adamo, C.; Jaramillo, J.; Gomperts, R.; Stratmann, R. E.; Yazyev, O.; Austin, A. J.; Cammi, R.; Pomelli, C.; Ochterski, J. W.; Martin, R. L.; Morokuma, K.; Zakrzewski, V. G.; Voth, G. A.; Salvador, P.; Dannenberg, J. J.; Dapprich, S.; Daniels, A. D.; Farkas, .; Foresman, J. B.; Ortiz, J. V.; Cioslowski, J.; Fox, D. J. Gaussian09 Revision D.01, Gaussian Inc. Wallingford CT. Gaussian 09 Revision C.01. 2010, p Gaussian Inc., Wallingford CT.

(21) Perdew, J. P.; Burke, K.; Ernzerhof, M. Generalized Gradient Approximation Made Simple. *Phys. Rev. Lett.* 1996, 77 (18), 3865–3868. <https://doi.org/10.1103/PhysRevLett.77.3865>.

(22) Hay, P. J.; Wadt, W. R. Ab Initio Effective Core Potentials for Molecular Calculations. Potentials for the Transition Metal Atoms Sc to Hg. *J. Chem. Phys.* 1985, 82 (1), 270–283. <https://doi.org/10.1063/1.448799>.

(23) Mosmann, T. Rapid Colorimetric Assay for Cellular Growth and Survival: Application to Proliferation and Cytotoxicity Assays. *J. Immunol. Methods* 1983, 65 (1–2), 55–63. [https://doi.org/10.1016/0022-1759\(83\)90303-4](https://doi.org/10.1016/0022-1759(83)90303-4).

(24) Chakraborty, S.; Mahadevan, B. K.; Shah, J.; Panse, K.; Malvi, B.; Balasubramanian, C.; Singh, S.; Misra, S. K. Enhanced Detection Using Stable Isotope Enriched <sup>65</sup>Cu Doped Ferrite Nanoparticles for Tracing Studies. *J. Alloys Compd.* 2020, 822. <https://doi.org/10.1016/j.jallcom.2019.153502>.



- (25) Misra, S. K.; Dybowska, A.; Berhanu, D.; Luoma, S. N.; Valsami-Jones, E. The Complexity of Nanoparticle Dissolution and Its Importance in Nanotoxicological Studies. *Sci. Total Environ.* 2012, 438, 225–232. <https://doi.org/10.1016/j.scitotenv.2012.08.066>.
- (26) Chakraborty, S.; Misra, S. K. A Comparative Analysis of Dialysis Based Separation Methods for Assessing Copper Oxide Nanoparticle Solubility. *Environ. Nanotechnology, Monit. Manag.* 2019, 12. <https://doi.org/10.1016/j.enmm.2019.100258>.
- (27) Mazurkow, J. M.; Yüzbaşı, N. S.; Domagala, K. W.; Pfeiffer, S.; Kata, D.; Graule, T. Nano-Sized Copper (Oxide) on Alumina Granules for Water Filtration: Effect of Copper Oxidation State on Virus Removal Performance. *Environ. Sci. Technol.* 2020, 54 (2), 1214–1222. <https://doi.org/10.1021/acs.est.9b05211>.
- (28) Weller, M. T.; Lines, D. R. Structure and Oxidation State Relationships in Ternary Copper Oxides. *J. Solid State Chem.* 1989, 82 (1). [https://doi.org/10.1016/0022-4596\(89\)90217-X](https://doi.org/10.1016/0022-4596(89)90217-X).
- (29) Wangpaichitr, M.; Wu, C.; You, M.; Maher, J. C.; Dinh, V.; Feun, L. G.; Savaraj, N. N<sup>1</sup>,N<sup>3</sup>-Dimethyl-N<sup>1</sup>,N<sup>3</sup>-Bis(Phenylcarbonothioyl) Propanedihydrazide (Elesclomol) Selectively Kills Cisplatin Resistant Lung Cancer Cells through Reactive Oxygen Species (Ros). *Cancers (Basel)*. 2009, 1 (1), 23–38. <https://doi.org/10.3390/cancers1010023>.
- (30) Lee, J. H.; Cho, Y. S.; Jung, K. H.; Park, J. W.; Lee, K. H. Genipin Enhances the Antitumor Effect of Elesclomol in A549 Lung Cancer Cells by Blocking Uncoupling Protein-2 and Stimulating Reactive Oxygen Species Production. *Oncol. Lett.* 2020, 20 (6). <https://doi.org/10.3892/ol.2020.12237>.

(31) Albayrak, G.; Korkmaz, F. D.; Tozcu, D.; Dogan Turacli, I. The Outcomes of an Impaired Powerhouse in KRAS Mutant Lung Adenocarcinoma Cells by Elesclomol. *J. Cell. Biochem.* 2019, 120 (6), 10564–10571. <https://doi.org/10.1002/jcb.28342>.

(32) Monk, B. J.; Kauderer, J. T.; Moxley, K. M.; Bonebrake, A. J.; Dewdney, S. B.; Secord, A. A.; Ueland, F. R.; Johnston, C. M.; Aghajanian, C. A Phase II Evaluation of Elesclomol Sodium and Weekly Paclitaxel in the Treatment of Recurrent or Persistent Platinum-Resistant Ovarian, Fallopian Tube or Primary Peritoneal Cancer: An NRG Oncology/Gynecologic Oncology Group Study. *Gynecol. Oncol.* 2018, 151 (3), 422–427. <https://doi.org/10.1016/j.ygyno.2018.10.001>.

(33) Gao, W.; Huang, Z.; Duan, J.; Nice, E. C.; Lin, J.; Huang, C. Elesclomol Induces Copper-Dependent Ferroptosis in Colorectal Cancer Cells via Degradation of ATP7A. *Mol. Oncol.* 2021. <https://doi.org/10.1002/1878-0261.13079>.

(34) Qu, Y.; Wang, J.; Sim, M. S.; Liu, B.; Giuliano, A.; Barsoum, J.; Cui, X. Elesclomol, Counteracted by Akt Survival Signaling, Enhances the Apoptotic Effect of Chemotherapy Drugs in Breast Cancer Cells. *Breast Cancer Res. Treat.* 2010, 121 (2), 311–321. <https://doi.org/10.1007/s10549-009-0470-6>.

(35) Du, Q.; Jia, W.; Dai, J.; Du, C.; Shao, A.; Zhang, R.; Ji, Y. Effect of Dissociation Constant (PKa) of Natural Organic Matter on Photo-Generation of Reactive Oxygen Species (ROS). *J. Photochem. Photobiol. A Chem.* 2020, 391. <https://doi.org/10.1016/j.jphotochem.2019.112345>.

(36) Raha, S.; Robinson, B. H. Mitochondria, Oxygen Free Radicals, Disease and Ageing. *Trends Biochem. Sci.* 2000, 25 (10), 502–508. [https://doi.org/10.1016/S0968-0004\(00\)01674-1](https://doi.org/10.1016/S0968-0004(00)01674-1).

- (37) Redza-Dutordoir, M.; Averill-Bates, D. A. Activation of Apoptosis Signalling Pathways by Reactive Oxygen Species. *Biochim. Biophys. Acta - Mol. Cell Res.* **2016**, *1863* (12), 2977–2992. <https://doi.org/10.1016/j.bbamcr.2016.09.012>.
- (38) Ahamed, M.; Siddiqui, M. A.; Akhtar, M. J.; Ahmad, I.; Pant, A. B.; Alhadlaq, H. A. Genotoxic Potential of Copper Oxide Nanoparticles in Human Lung Epithelial Cells. *Biochem. Biophys. Res. Commun.* **2010**, *396* (2), 578–583. <https://doi.org/10.1016/j.bbrc.2010.04.156>.

## LIST OF FIGURES

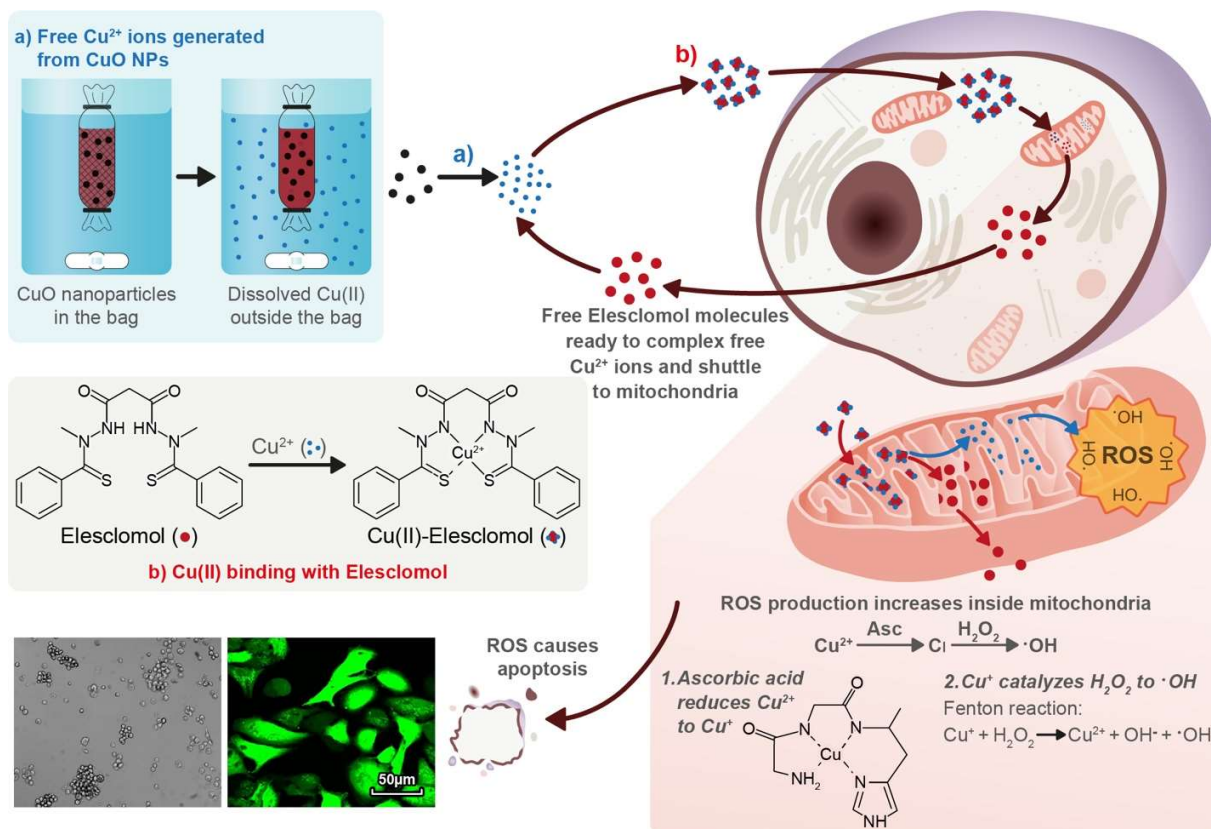


**Figure 1:** Schematic showing dissolved  $\text{Cu}(\text{II})$  binding to free Elesclomol and forming  $\text{Cu}(\text{II})$ -Elesclomol complex and mechanism of ROS generation once Elesclomol delivers  $\text{Cu}(\text{II})$  ions inside mitochondria.

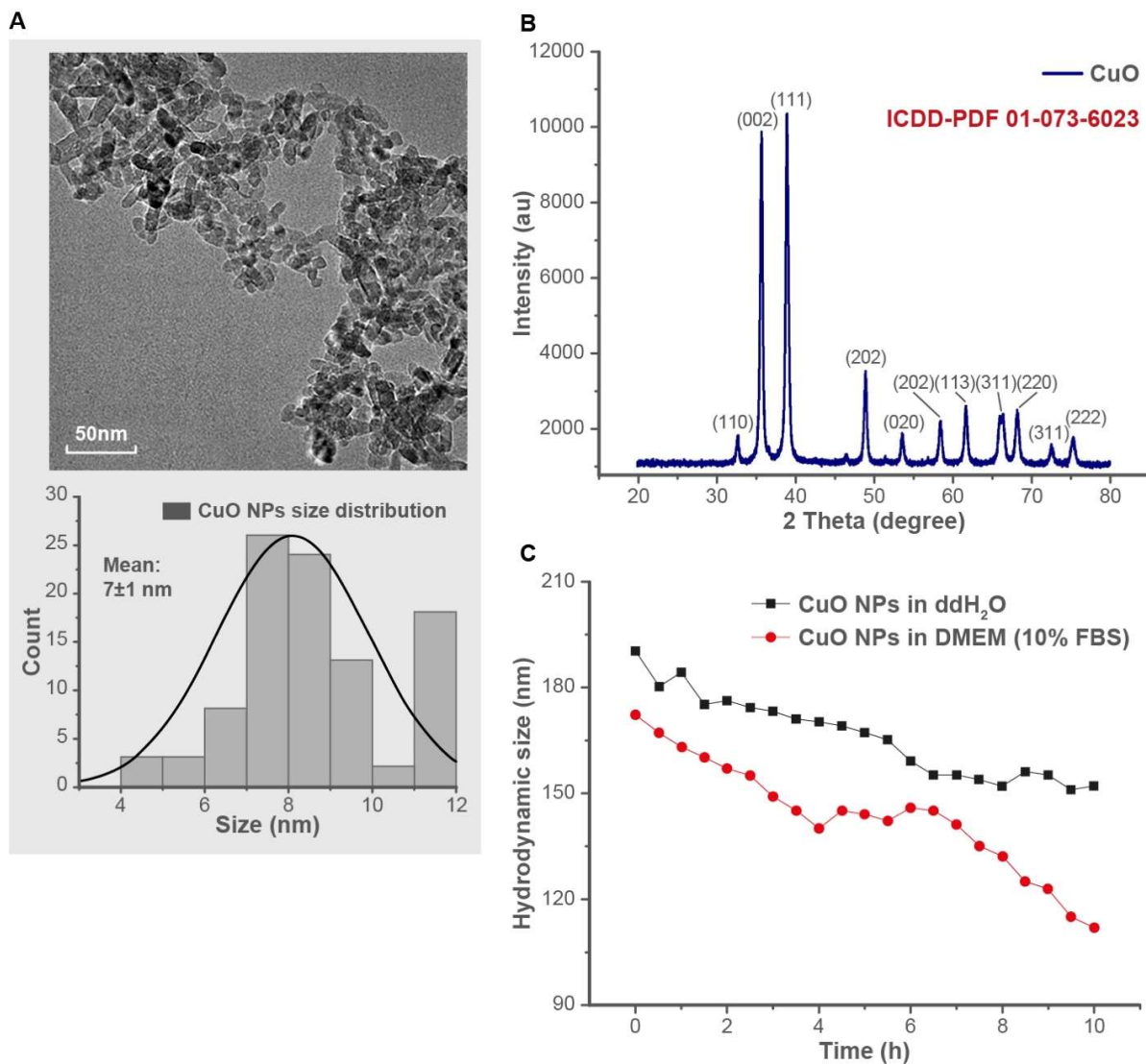


**Figure. 2:** Characterization and stability studies of CuO nanoparticles (A) TEM image and size distribution of CuO nanoparticles (number of particles=100), (B) X-ray diffractogram of CuO nanoparticles (C) Suspension stability of CuO nanoparticles in DMEM media and in deionized water.

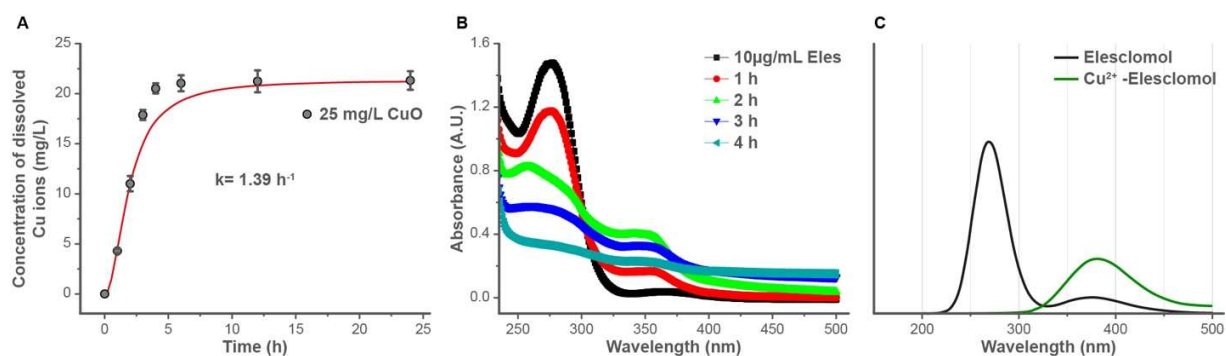


**Figure. 3** (A) Dissolution profile of CuO nanoparticles in DMEM media, (B) CuO dissolution mediated Elesclomol-copper ions complex formation at different time points. (C) Theoretical UV-vis spectra from DFT calculations showing a  $\lambda_{\text{max}}$  of 275 nm for Elesclomol and  $\lambda_{\text{max}}$  of 380 nm for Cu(II)-Elesclomol complex.

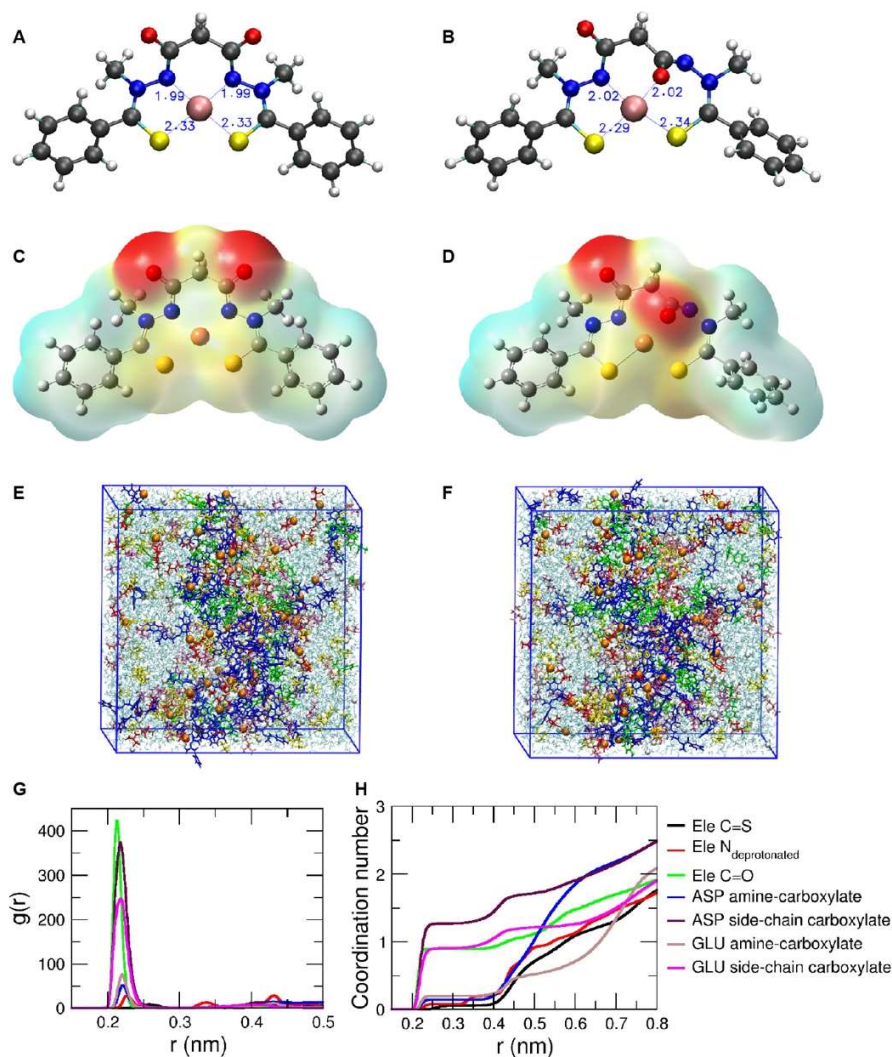


**Figure. 4** Optimized geometries (A) GM1 and (B) GM2 of Cu (II)-Elesclomol complex obtained from PBE/LanL2DZ&6-31+G(d,p) DFT calculations; (C) GM1 and (D) GM2 show the electrostatic potential mapped on the electron density obtained from DFT calculations. Snapshots from classical MD simulation under NVT ensemble conditions at (E)  $t = 20$  ns, (F)  $t = 30$  ns.: Orange (balls) – Cu(II), white (balls) – Na<sup>+</sup>, Cyan, transparent (sticks) – water, blue (sticks) – Elesclomol, {red, pink, magenta, yellow, green} (sticks) – amino acids. (G) Radial distribution and (H) coordination number of various Elesclomol and amino acid binding sites around Cu (II) from  $t = 10$  ns to  $t = 30$  ns from the production run under NVT conditions.

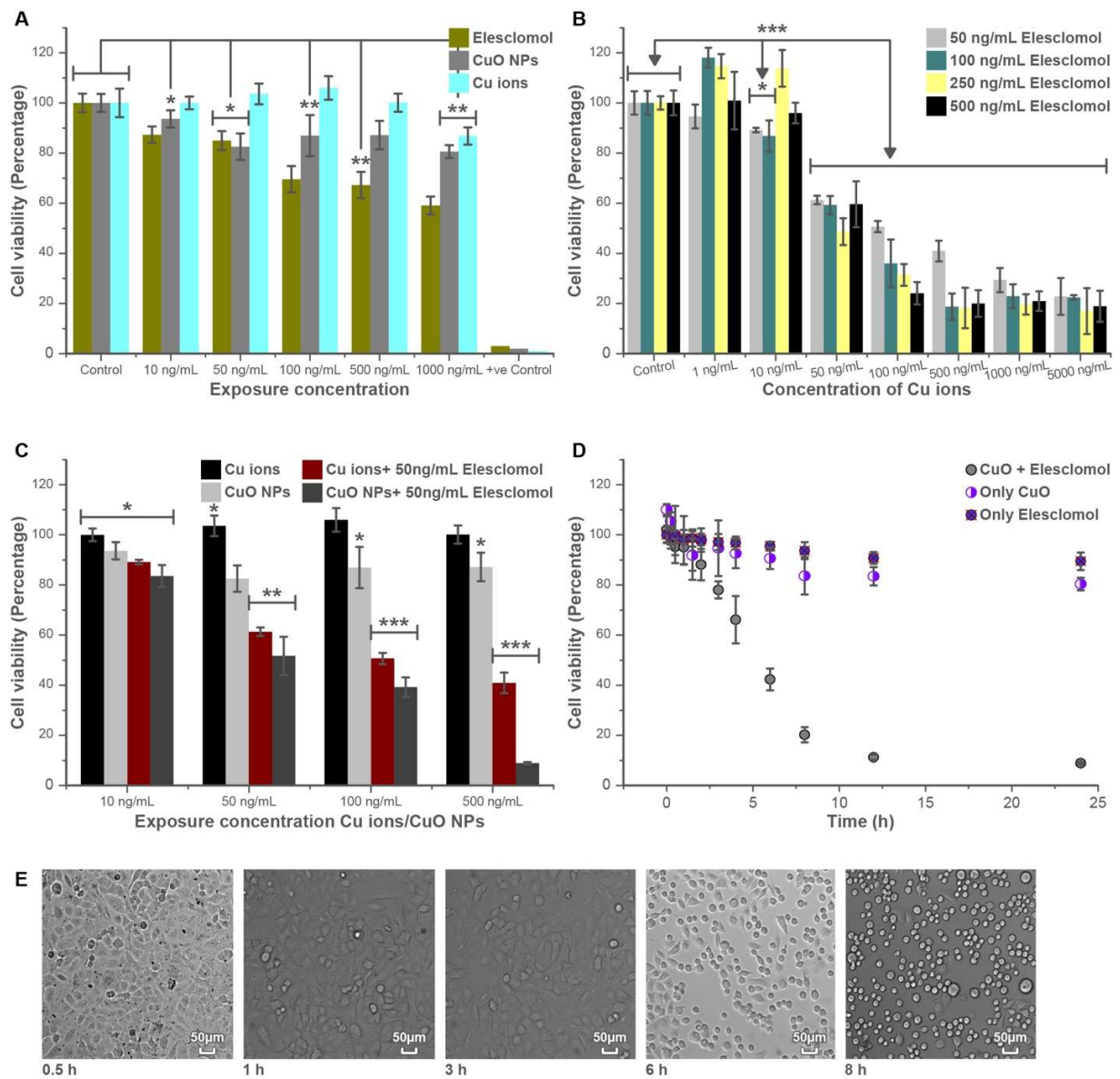


**Figure. 5** Cytotoxicity study in A549 cells after 24 h of incubation with (A) varying concentrations of Elesclomol, Cu ions and CuO nanoparticles, (B) Cu ions in a range of concentration with Elesclomol (C) Cu ions, CuO nanoparticles, Cu ions + Elesclomol, and CuO nanoparticles + Elesclomol. (D) Time dependent cell viability measurement of A549 cells upon exposure to of Elesclomol (50 ng/mL), CuO nanoparticles (500 ng/mL), and CuO nanoparticles (500 ng/mL) +



Elesclomol (50 ng/mL). (E) The morphology of A549 cells are shown at selected time point after the exposure of to CuO nanoparticles (500 ng/mL) + Elesclomol (50 ng/mL).

(Data presented as mean±standard deviation (n=3). \* $p < 0.05$ , \*\* $p < 0.01$ , \*\*\* $p < 0.001$ , \*\*\*\* $p < 0.0001$ . The absorbance was recorded at 590 nm and the viability of untreated control cells was considered as 100%. The statistical analysis was done compared to control.

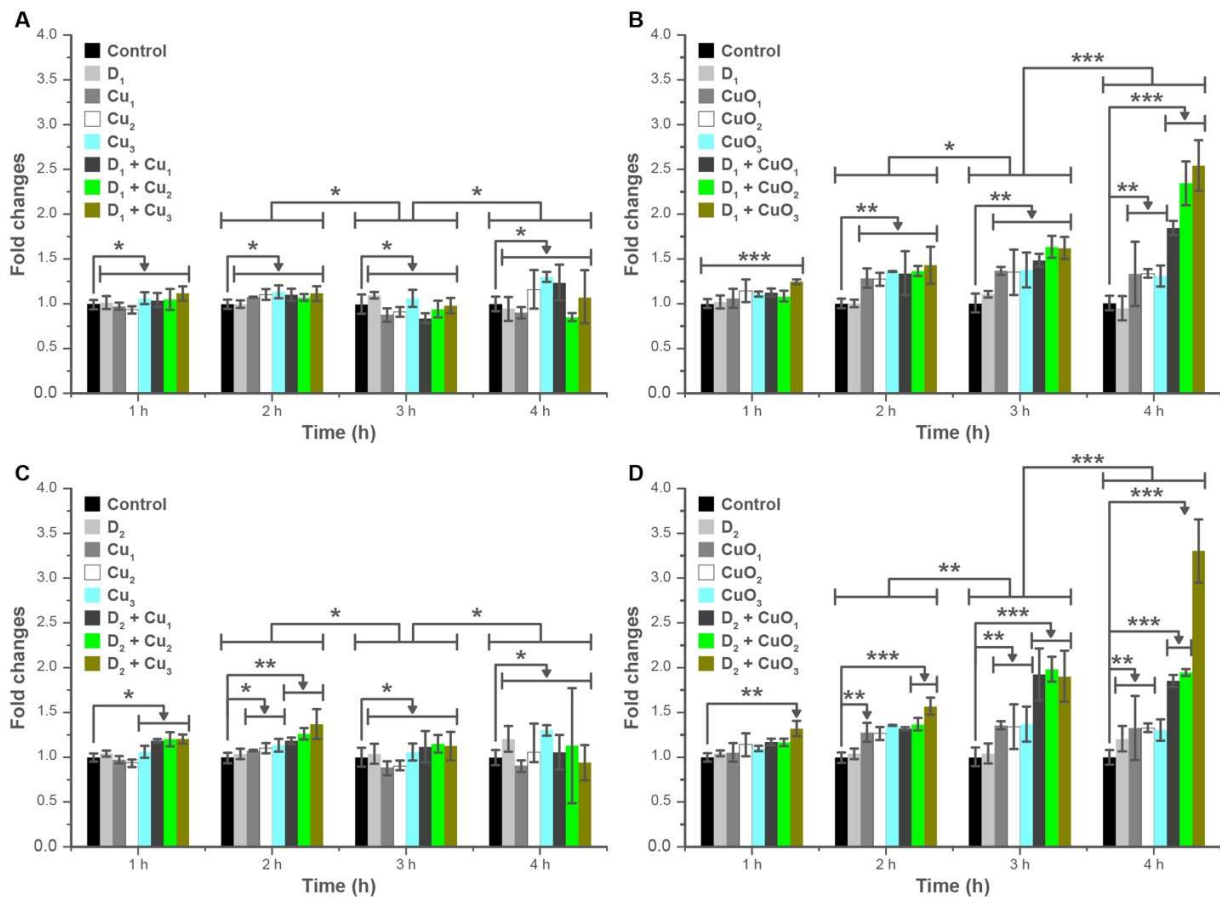


**Figure. 6** ROS generation on A549 cells exposed to different concentration of Cu ions, CuO nanoparticles, drugs followed by DCFDA exposure for 30 min. (A) ROS generation on exposure to Cu ions and Elesclomol (10 ng/mL) combinations, (B) ROS generation on exposure to CuO

nanoparticles and Elesclomol (10 ng/mL) combinations. (C) ROS generation on exposure to Cu ions and Elesclomol (50 ng/mL) combinations, (D) ROS generation on exposure to CuO nanoparticles and Elesclomol (50 ng/mL) combinations. The ROS generation was measured by fluorescence spectrophotometer and data represented in fold change compared with control. Data represented as mean  $\pm$  standard deviation (n=3). \*p<0.05, \*\*p<0.01, \*\*\*p<0.001.

Nomenclature- D<sub>1</sub>: 10 ng/mL Elesclomol, D<sub>2</sub>: 50 ng/mL Elesclomol, Cu<sub>1</sub>: 50 ng/mL, Cu<sub>2</sub>: 100 ng/mL, Cu<sub>3</sub>: 200 ng/mL, CuO<sub>1</sub>: 50 ng/mL, CuO<sub>2</sub>: 100 ng/mL, CuO<sub>3</sub>: 200 ng/mL

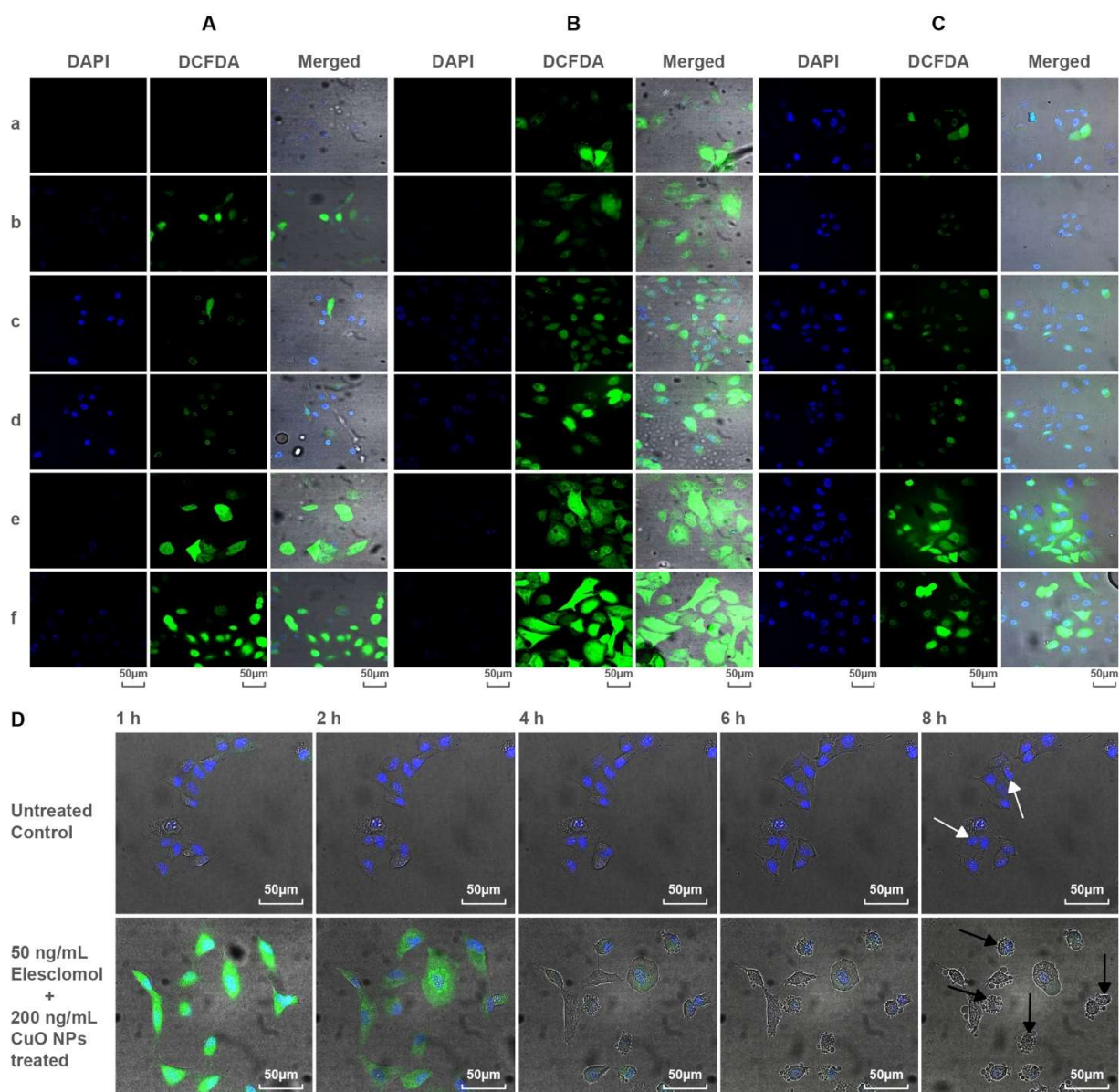


**Figure 7:** Pictomicrograph showing the time dependent ROS production by A549 cells at 50 ng/mL of Elesclomol and two different concentration of CuO nanoparticles (100 ng/mL and 200 ng/mL) (A) Time = 1 h, (B) Time = 2 h (C) Time = 3 h. (Blue dye represents DAPI, Green dye represents DCFDA). (D) Live cell imaging snapshots collected from live cell video (SI video files) showing the A549 cells undergoing apoptosis after the end of 8 h of exposure to Elesclomol (50 ng/mL) + CuO nanoparticles (200 ng/mL) (Blue dye represent Hoechst, Green dye represents

DCFDA). The black arrow indicators represent A549 cells undergone apoptosis and white arrow indicators represents healthy A549 cells

Legend nomenclature - a: Control, b: 50 ng/mL Elesclomol, c: 100 ng/mL CuO nanoparticles, d: 200ng/mL CuO nanoparticles, e: 50 ng/mL Elesclomol + 100 ng/mL CuO nanoparticles, f: 50 ng/mL Elesclomol + 200 ng/mL CuO nanoparticles.

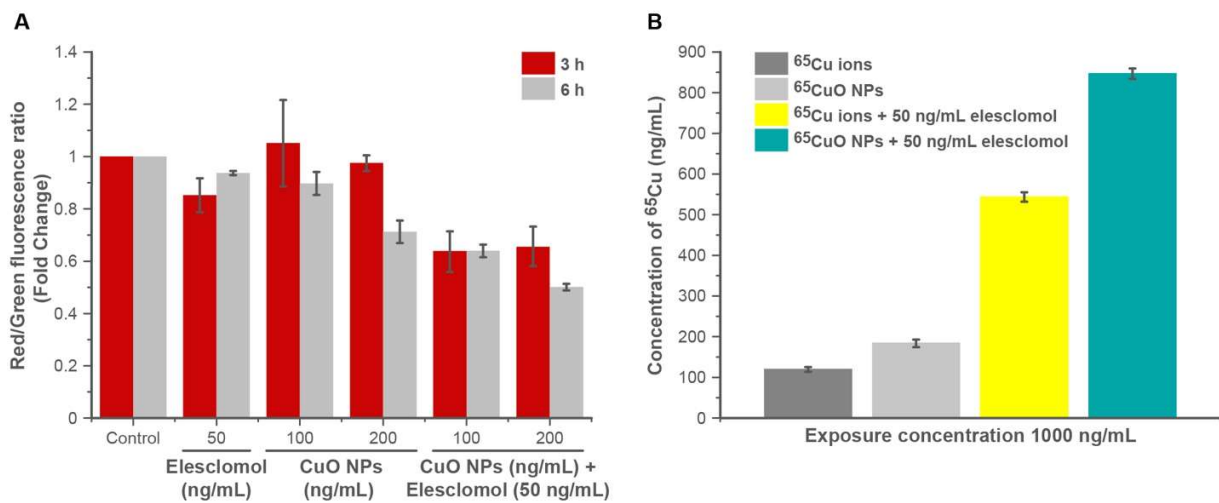


**Figure 8:** (A) Mitochondrial membrane potential assay showing decreased fold change in Red/Green fluorescence ratio on exposure of CuO nanoparticles + Elesclomol. (B) Accumulation of <sup>65</sup>Cu in A549 cells on exposure of 1000 ng/mL <sup>65</sup>Cu ions and <sup>65</sup>CuO nanoparticles with or without 50 ng/mL Elesclomol for 3 h. Data represented as mean ± standard deviation (n=3).

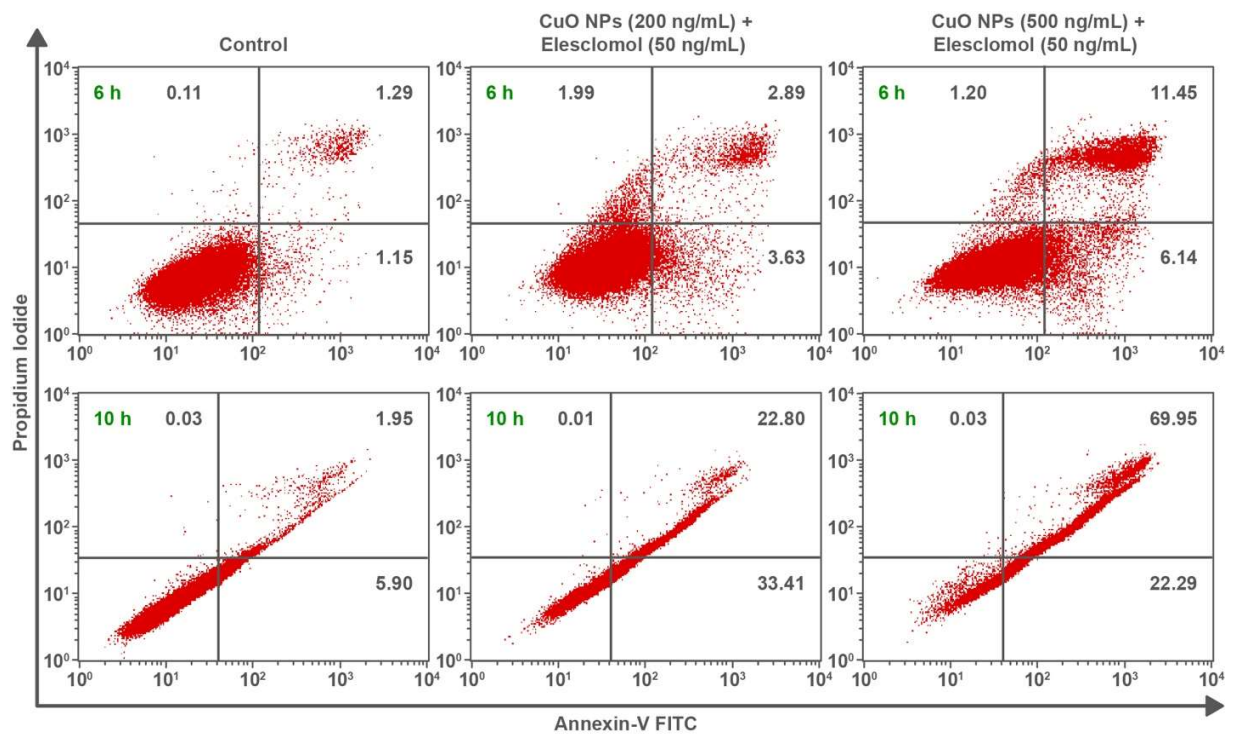


**Figure 9:** Time dependent apoptosis/necrosis in A549 cells exposed to Elesclomol, CuO nanoparticles and CuO nanoparticles co-delivered with Elesclomol. Dot plot analysis of apoptotic cells by the annexin-V/PI staining after 6 h and 10 h treatment. Data represented as mean  $\pm$  standard error calculated from two individual experiment (n=2).

### TOC graphics

